CHARA on-sky beam stabilization with automated beam guiding

Narsireddy Anugu, Matthew D Anderson, Theo A ten Brummelaar, Julien Dejonghe, Christopher D Farrington, Douglas R Gies, Jeremy W Jones, Rainer Kohler, Stefan Kraus, Cyprien Lanthermann, E Robert Ligon, Olli Majoinen, John D Monnier, Denis Mourard, Stephen T Ridgway, Gail H Schaefer, Nicholas J Scott, Judit Sturmann, Laszlo Sturmann, Nils H Turner, Norman L Vargas

Abstract. CHARA is the longest baseline optical interferometer in the world. The ambitious sensitive and accurately calibrated science observations require robust automated beam stabilization operations. In this report, we summarize the auto-alignment system that is in operation at the CHARA. We discuss the advantages and disadvantages of the system, outline new improvements that are considered to implement, and summarize lessons learned through daily operations at the CHARA Array.

Keywords: Optical interferometry.

*Narsireddy Anugu, nanugu@gsu.edu

1 Introduction

The Center for High Angular Resolution Astronomy (CHARA) Array[1] is the world's longest-baseline optical interferometer. It combines six telescope beams separated by hundreds of meters and delivers (sub)milliarcsecond angular resolutions. One of the challenges of the operation of the array is the beam transport from the telescope to the entrance of the beam combiner while preserving the beam angular offset and pupil shear within science requirements.

The main science drivers of the CHARA Array are imaging extended objects, detecting binaries and their astrometry, and measuring stellar diameters. These science cases push for (i) highly sensitive observations, (ii) accurate visibility calibrations, for example, imaging extended objects and measuring diameters,[2] and (iii) astrometric measurements requiring pupil stabilization throughout the observations.[3,4] As turns out that beam stabilization is crucial as any errors in the beam angle and pupil position would provoke fringe visibility loss in interferometric measurements.

CHARA is equipped with next-generation beam combiners: Silmaril (CLASSIC upgrade; H+K-bands),[5] MIRC-X (J+H-bands),[6] MYSTIC (K-band)[7] and SPICA (R-band).[8] The science drivers of each instrument can be found in their respective papers. These instruments are designed to take advantage of the adaptive optics corrected star injection into respective instruments. An efficient flux injection into the single-mode fibers requires stabilization of beam < 180 mas angular offset error < 0.5 PSF, and $< 1\%$ or < 0.2 mm pupil shear.

This report is organized as follows. An overview to the systems involved at CHARA Array relevant to the alignment problem are described in Section 2. The alignment problem and beam stabilization requirements to achieve the science goals are reported in Section 3. The Section4 and Section 5 summarizes the daytime and on-sky automated alignments. We discuss the performance of CHARA with contemporary interferometers and outline the future improvements in Section 6. The final section gives the conclusions.

2 The CHARA system overview

Before going to the specifics of the alignment problem, let's introduce the CHARA Array briefly that are relevant to this study. CHARA Array is equipped with adaptive optics (AO) systems at the telescope (TELAO) and in the beam combiner lab (LABAO). The design, construction, and operation of TELAO and LABAO are extensively documented elsewhere.[9–13]

2.1 Telescope adaptive optics (TELAO)

The specifications of the TELAO are tabulated in Table 1 and 2. The TELAO is designed to correct the atmospheric turbulence above the telescope and improve the Strehl ratio of the beams in H or higher wavelengths. In a statistical average, TELAO delivers a 50% Strehl ratio in H-band wavelengths. Each TELAO system consists of (a) a 7×7 lenslet-based Shack-Hartmann wavefront sensor, (b) a sub-electron readout noise, Andor 897 EMCCD camera to record the Shak-Hartmann sensor images, and (c) an ALPAO voice-coil based deformable mirror with 61 actuators. The TELAO DMs are placed in the position of the M4 mirror to limit new reflections to the beam train.

Table 1 TELAO and LABAO wavefront sensor specifications

Parameter	TELAO	LABAO
Lenslet sub-apertures	7×7	6×6
Effective sub-apertures	36	32
Sub-aperture field of view	6.7″	4.6″
Pixel per sub	9	5
camera window size	90×90	160×128
Frame rate	500Hz	100Hz
Sensitivity R-band	< 14 with EMCCD gain	< 4
Zernikes measured	21	21

2.2 Telescope Dichroic (TELDICH)

The TELAO has three dichroic glasses to optimize the science observations at different wavelengths spanning R-band to K-band wavelengths: BARE, VIS, and YSO. Based on a science requirement, an appropriate dichroic filter is chosen to maximize flux into the TELAO WFS. Table 3 presents the dichroic filter and their percentage of share into the TELAO WFS. All the near-infrared light enters the beam combiner lab.

- The TELDIC has its coating on the upper surface.
- The blue beacon crosses the TELDIC, is reflected by the coating, and crosses a second time the TELDIC.

- A major part of the red beacon is transmitted through the TELDIC to the TWFS and is thus affected by the wedge of the TELDIC.
- The other part of the red beacon (only a few % in the case of the YSO TELDIC) follows the same path of the blue beacon but with a differential chromatism effect.
- The TELDIC reflects a part of the visible band to the TWFS. The wedge of the TELDIC does not have any impact on this beam.
- The rest of the visible band and the infrared are transmitted to the Lab through the TELDIC. This beam is dispersed because of the wedge of the TELDIC (5arcmin as measured, 3arcmin in specifications).

Table 2 The TELAO and LABAO deformable mirror specifications

Parameter	TELAO	LABAO
DM actuators	ALPAO 61	OKO MMDM 37
Size	18cm	15 mm
Inter-actuator stroke	4μm	0.5μm
First resonance	500 Hz	-
Settling time	2ms	-
Mirror best flat	$<$ 30 nm	400 nm
r_0	$\sim$ 5cm at 0.5μm, 21cm at 1.6μm	

Table 3 TELAO dichroic filter selection and % light shared with the TELAO WFS

Dichroic glass	% of visible light share to TELAO WFS
BARE	4%
VIS	20%
YSO	100%

2.3 Laboratory adaptive optics (LABAO)

The LABAO is installed in the beam combiner laboratory and is designed to correct the residual atmospheric turbulence errors and also the laboratory seeing as the lab is filled with air more than 50 meters. The LABAO systems were built cost-effectively by using off-the-shelf DM (OKO MMDM with 37 actuators) and 6×6 lenslet imaged with Thorlabs DDC1545M USB camera. The specifications of the LABAO are tabulated in Table 1 and 2.

To boost the sensitivity of the LABAO, we use the calibrated beacon source from the telescope. A blue beacon light at $\lambda = 465$ nm is used for this purpose. A multimode fiber emits this blue

beacon light, which is expanded and collimated by an on-axis parabolic mirror (d = 152.4 mm, f = 1219.2 mm). A flat mirror directs the collimated beam toward a telescope dichroic splitter. In reflection of TELDICH, the beam passes through the beam relay and delay lines to the wavefront sensor of the LABAO. From the same blue beacon fiber, there also emits a red beacon, which is used for aligning the TELAO wavefront sensor. The red beacon reaches the TELAO wavefront sensor via TELDICH transmission.

LABAO is the wavefront reference for all the beam combiner instruments.

2.4 Six Telescope Star Tracker for near-infrared (STST)

The Six Telescope Star Infrared Tracker (STST) was installed in the beam combiner lab to monitor the near-infrared star beams. The STST tracks beam angular offsets (tip-tilt; $[x, y]$) and pupil (later offsets; $[Px, Py]$) by imaging the six telescope beams on the C-RED 2 camera from the First Light. The STST is used to track the star tilt in the lab as the LABAO only works in the visible. The full description of the STST can be found in CHARA technical report[1].

2.5 SPICA star tracker

The SPICA star tracker is inbuilt in SPICA.[8] The SPICA star tracker tracks beam angular offsets and pupil shear for the six telescope beams. SPICA has also internal pupil and image centering capabilities.

3 The beam alignment problem and beam stabilization requirements

As mentioned in the Introduction 1, in practical conditions, achieving the beam stabilization requirements (beam angular offset error $<$ 180 mas or half of AO corrected PSF and $<$ 1% or $<$ 0.2 mm pupil shear) is challenging for the following reasons.

- Atmospheric differential refraction (ADR): The refraction of starlight through the atmospheric dispersion at different wavelengths leads to differential photo-centers imaged on the detector. A common solution, which is found in modern telescopes is the Atmospheric Dispersion Compensator (ADC). This is not implemented at the CHARA telescopes in the interest of the throughput of the system as it adds extra 4 air-glass dioptric surfaces (two Risley prisms) and cost.
- TELDICH wedge: In addition to the atmospheric refraction, the telescope dichroic (5 arcminute one wedge) and vacuum window (2 wedges) create additional differential refraction between the visible beam and the infrared beam. Ideally, the two vacuum windows have been set to cancel the dispersion but in practical terms there is residual dispersion and associated refraction.

[1] STST manual

- Optomechanical drifts: The CHARA array consists of 20 mirrors from the telescope to the entrance of the beam combiner, including moving delay lines. The beam is transported around hundreds of meters, any small unaligned optomechanical drift creates beam angular offset and pupil shear at the entrance of the beam combiner.

- Temperature fluctuations: The beam relay optics that deliver light from the telescope to the laboratory are inevitably exposed to outdoor temperatures and seasonal temperature cycles, leading to significant beam alignment drifts over timescales of minutes.

Since the blue beacon is being used for the LABAO, effectively the photo center of the blue beacon wavelength reaches the entrance of the beam combiner. Due to dispersion caused by passing the beam through atmospheric air, TELDICH wedge and transmissive optics, the photo center seen at visible wavelengths is very far away at near-infrared wavelengths.

3.1 Beam angular offsets

We computed (see Figure 1) that the differential refraction for $z = 60°$, between 0.5μm (blue beacon on LABAO) and 2.4μm (K band for MYSTIC) is 1.6″ on sky. This number goes down to 0.77″ between 0.7 and 2.4μm. Adding this refraction to the field rotation, in the case of a non-centered beam, will probably generate vignetting following your 0.7″ margin, of course for the longest pipes. For H band, these numbers are 1.5″ (0.5-1.6 μm) or 0.68″ (0.7-1.6 μm). All the atmospheric refraction computations were made at elevations at 60°, which is usual for the Southern young stellar object targets.

Figure 2 shows visually the refraction difference of LABAO wavelength and H-band MIRC-X wavelengths.

The on-sky refraction tests with the STST shows that we measure a total of 3 arcsec, which is $\sim 5 - 10\times$ larger than the unvigneted field of view of the CHARA $(0.3 - 0.6)''$.

The path length from the telescope to the beam compressor will be about 100 meters. The apparent shear between wavelengths of 0.465 nm and 1.7 μm is found by multiplying these distances by the angles associated with the nominal beam diameter, giving the final answer of 9.0 mm (out of 19 mm size at the entrance of MIRC-X beam combiner), which is around 45% lateral pupil shift.

To quantify the effects of refraction, we carried out the following experiments of measuring the offset of IR light on the Star Tracker at different telescope pointings. We co-aligned the lab to the LABAO and STST (see Section 4). The standard alignment sequence was used to align the blue and red beacons at each pointing. The cal source was then centered on the TELAO. The results are shown in Figure 3. We measured VIS-IR photo-center offset to a calibrated source inside the telescope and on-sky star to differentiate the contributions from the TELDICH and atmospheric turbulence. We see an expected rotation of IR photo-center on the STST with azimuth.[14] When rotating the telescope in azimuth, the wedged dichroic is rotating with respect to the lab. We conclude that the inner radius of the on-sky ring is likely caused by dispersion from the TELDICH

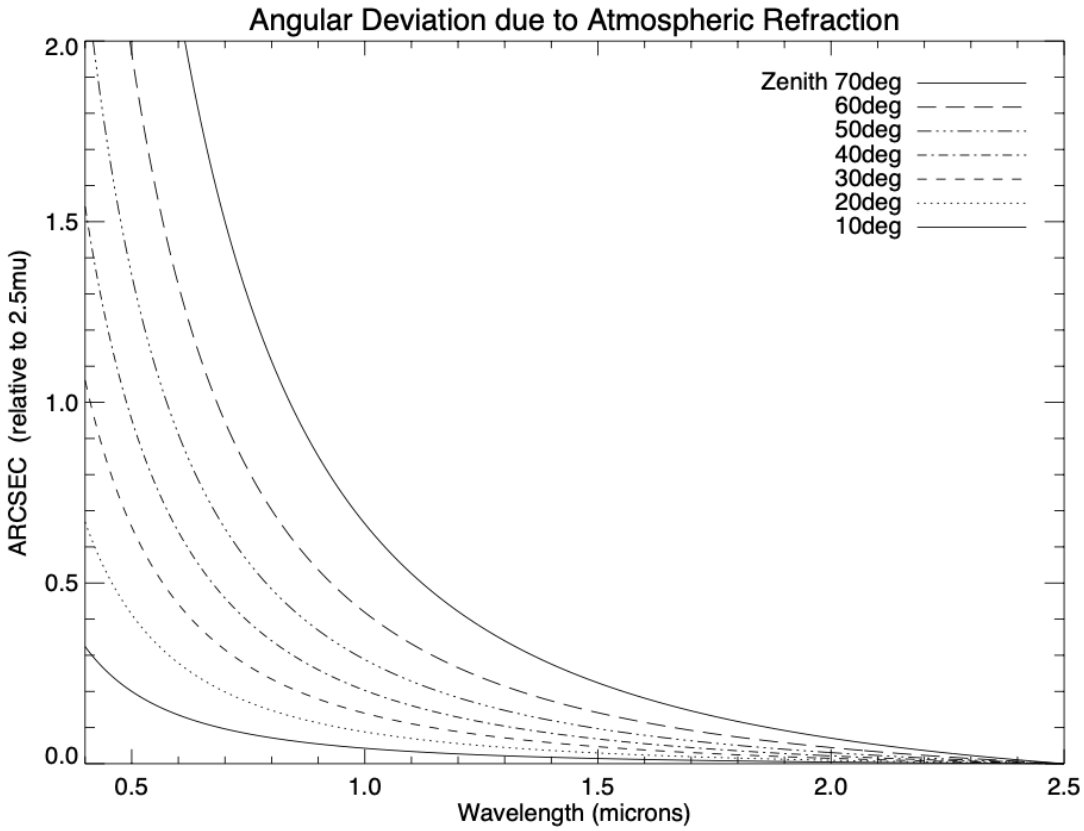

Fig 1 Atmospheric refraction angle with reference to K-band $\lambda = 2.5\mu$m.

(Figure 3 left panel) and the width of the on-sky ring is caused by atmospheric refraction (elevation-dependent).

Figure 4 shows the Zemax simulations (Thanks to Julien) of how the beam pupil is laterally shifted and tilted. A 3.4 mm shift out of the 19 mm beam is (18%) laterally shifted for the 465nm to 1700nm differential wavelengths. A 0.6 angular beam offset ($1 - 2\times$ the CHARA field of view) was measured for the (465nm to 1700nm) differential wavelengths.

3.2 Beam pupil shear and AO performance degradation

Thanks to Julien for computing the refraction effects of TELDICH wedge using Zemax. Figure 5 shows the lateral pupil shift between the LABAO beacon reference wavelength (465nm) to MIRC-X (1700 nm) and that is 0.8 mm for the LABAO Deformable Mirror (beam diameter 10.5 mm). This is 8% for the TELDICH wedge angle (5 arcminutes) only. Considering the atmospheric refraction, which is almost equal or more to the TELDICH wedge refraction (see Figure 3), the pupil later shift becomes $2 \times 8\%$ or more.

This 16% lateral pupil shift amounts to one sub-aperture shift on the LABAO or vignetting of the pupil by one LABAO sub-aperture. This means that the wavefront corrections measured at LABAO wavelengths are not appropriate for the IR wavelengths as there is pupil misregistration

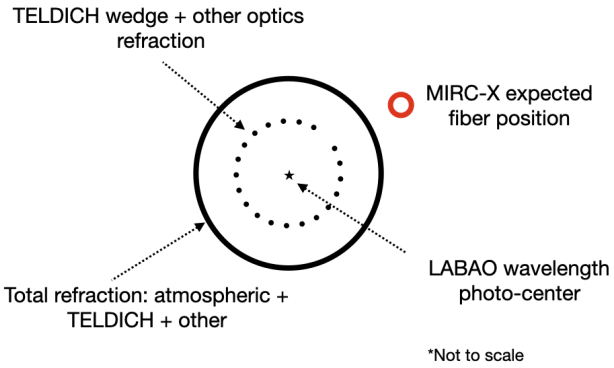

Fig 2 A schematic view of the refraction problem seen between the LABAO beacon reference wavelength and the near-infrared beam combiner (e.g., MIRC-X). The position of the beam arriving at the lab will depend on the wavelength; the recorded intensity will be stretched to a ring due to telescope azimuth rotation. The "⋆" symbol is the location of the photo-center of flux at the LABAO 465nm wavelength. The MIRC-X fiber at 1700nm is aligned to the CHARA lab reference, STS but its starlight photo-center is away from the LABAO photo-center reference. The location of the smaller (dotted) ring is the photo-center of the IR beam due to the TELDICH wedge angle and other optical transmissions. The location of the larger ring (thick line) is the photo-center of the IR beam due to the total refraction including the atmosphere. The refraction rotation is due to the azimuth. The refraction amplitude changes with the telescope elevation. However, we see a rotation with azimuth, suggesting dispersion between visible and IR light caused by the dichroic mounted on the AOB. The radius of the ring that is traced out is similar to the inner radius we see in the on-sky observations. The position of the beam arriving at the lab will depend on wavelength; the recorded intensity will be stretched to an ellipse.

with respect to the DM. This misregistration of pupils accounts to 20-30% drop of the Strehl ratio in H-band wavelengths.

As mentioned above, the misalignment in beam angle (tilt) and beam position (shear) reduces the signal-to-noise ratio of interferometric science measurements. In the coarsest sense, the beam profile becomes obstructed by apertures within the beam train, thereby losing flux due to vignetting. When it comes to combining the beams, this loss is unlikely to be matched between beamlines, so fringe contrast will be reduced. In order to stabilize these beams we needed an accurate automatic alignment system.

Table 4 presents the misalignments before the corrections and goals to achieve improved sensitivity.

Table 4 Beam misalignments before the alignments and goals to achieve with the auto-alignment

Parameter	Before alignment	Goals
Beam tip/tilt	3″	180 mas (0.5× AO corrected PSF)
Pupil lateral shift at LABAO	16% pupil	< 1% pupil
Pupil lateral shift at MIRC-X	45% pupil	< 1% pupil

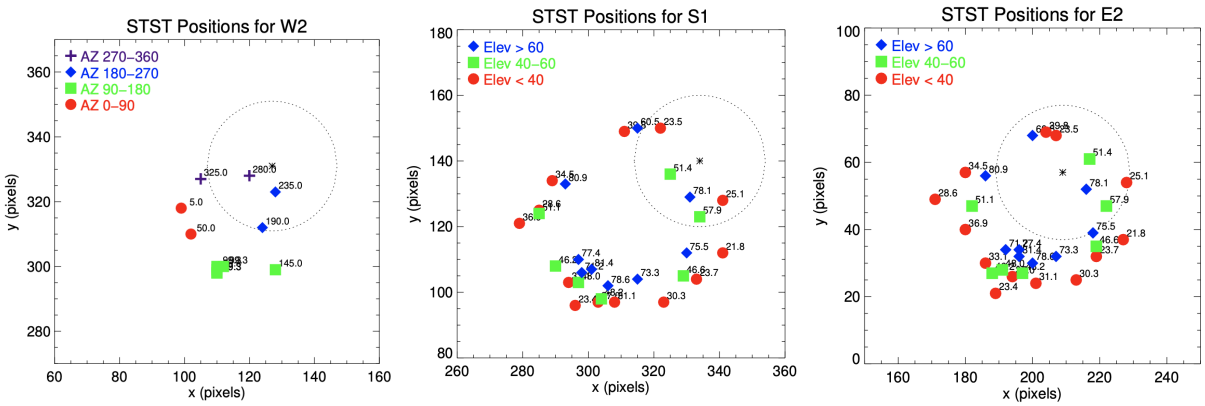

Fig 3 The refraction effects recorded on the STST near-infrared camera. (Left panel) The differential wavelength refraction from the TELDICH wedge angle. A cal source was injected from the telescope and a near-infrared photo-center was recorded as a function of the telescope azimuth. (Middle panel) The total refraction observed for an on-sky target with an S1 telescope. (Right panel) Same as the middle panel but an E2 telescope. The circle of rotation of the photo center seen on the STST is due to the azimuth. The asterisk marks the position of the Six Telescope Simulator (STS) with 1 radius of the dotted circle. The symbols are color-coded according to elevation and azimuth.

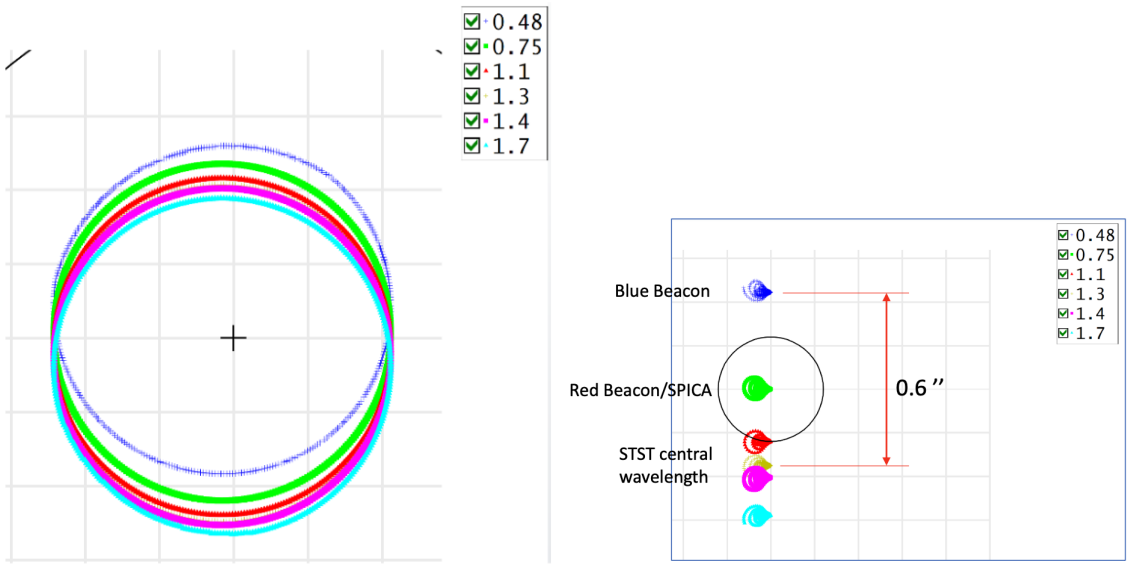

Fig 4 TELDICH wedge resulting refraction effects. (Left panel) A 3.4 mm out of 19mm beam size (18%) pupil lateral shift was measured at the STST for the (465nm to 1700nm) differential wavelengths. (Right panel) A 0.6 angular beam offset (1 − 2× the CHARA field of view) was measured for the (465nm to 1700nm) differential wavelengths at the STST. See, See, Julien Dejonghe email thread 2023Feb08.

Fig 5 (Left panel) We measure around 16% pupil shift at the LABAO due to atmospheric refraction and wedge of the angle of the dichroic from 465 nm to 2200 nm. That is almost equal to the one sub-aperture shift on the LABAO or vignetting of one sub-aperture. (Right panel) The 16% pupil implies that the K-band beam misaligned more than a sub-aperture in comparison to the blue wavelength pupil aligned on the LABAO. See, Julien Dejonghe email thread 2023Feb08.

4 Alignment strategies and daytime alignments

The daytime alignment concepts are described in detail in Technical Report 104[2]. Here we summarize.

4.1 Co-alignment of TELAO and LABAO

The co-alignment of the TELAO and LABAO systems is solved by generating blue (465 nm) and red collimated beacon (780 nm) beams from a single fiber and these beacons are used to co-align the two adaptive optics systems (red beacon – TELAO; blue beacon LABAO). At the TELDICH, the blue beacon reflects and travels downstream to the LABAO. The red beacon transmits through the TELDICH and reaches the TELAO. Figure 6 presents the spectral response of the TELAO, LABAO, and STST.

The initial alignment consists of aligning and focusing the blue beacon (465 nm) on the reference boxes of the LABAO (focus of beacon + telescope Dichroic) and at the same time of aligning and focusing the red beacon (780 nm) on the TWFS by adjusting the feeding optics of the TWFS.

4.2 Co-alignment of beam combiners with TELAO and LABAO using the alignment green fiducial laser

The CHARA optical axis is defined by a green (532 nm) laser in the beam combination laboratory. When this lab green laser is directed downstream, the fiducial laser helps to align beam combiners and the STST. When directed upstream through the relay pipes toward the telescope, the fiducial shares the same diameter as the stellar beam (i.e. 125 mm). A retractable corner cube retroreflector

[2]TR 104, Alignment Maintenance Task List for Daytime, J. Sturmann

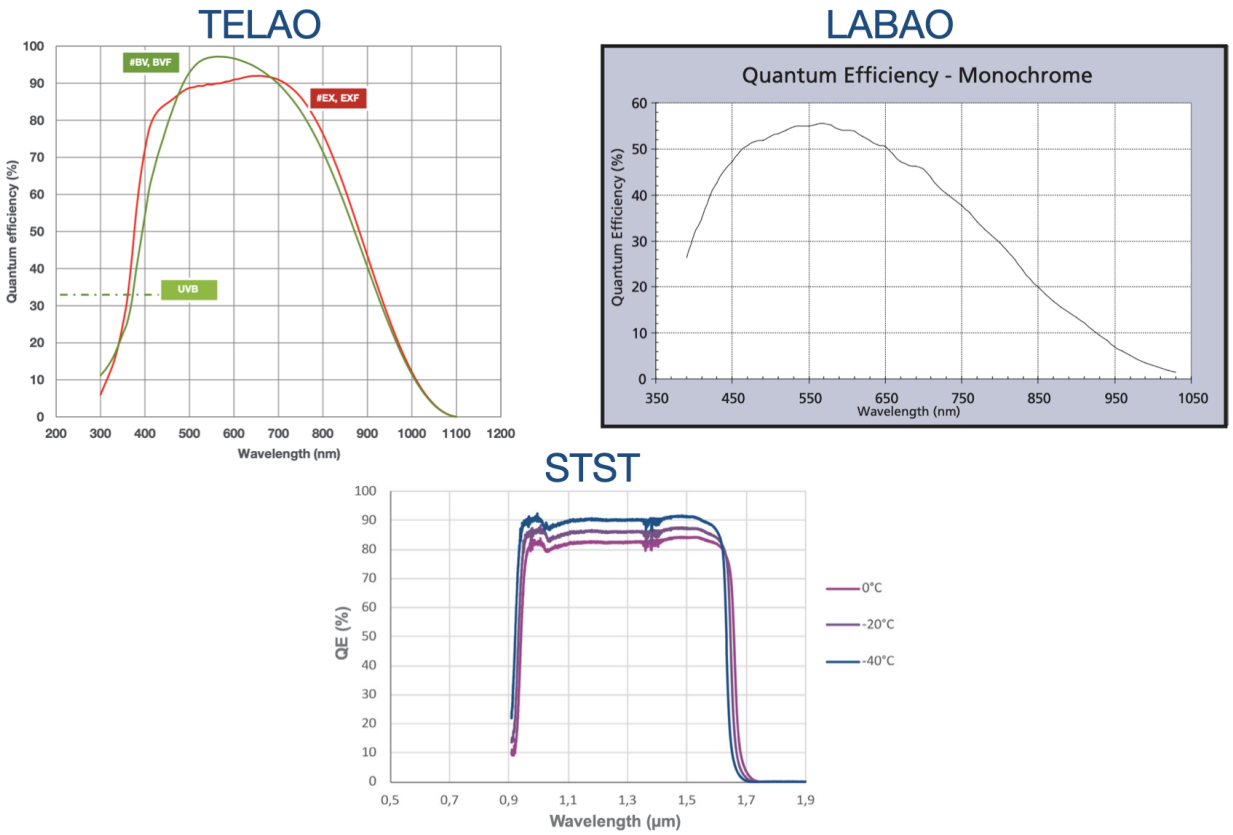

Fig 6 Spectral response of the TELAO, LABAO and STST cameras.

in front of M2 sends the beam back so that it can be recorded on the acquisition camera at the telescope table. When observing a stellar target, the telescope pointing is adjusted until the target spot overlaps with the laser spot on the acquisition readout.

4.3 Six Telescope Simulator in near-infrared at the lab (STS)

The Six Telescope Simulator (STS) is installed in the lab, which is co-aligned and co-phased (Optical path difference) with the CHARA alignment laser. STS provides 6 collimated beams of broadband light and is used to calibrate all the beam combiner instruments and co-phase each other in OPD terms.[6] The concept is similar to ARAL and the GRAVITY Calibration Unit at the VLTI.

5 On-sky auto alignment solution

5.1 Why automated alignment?

The manual refraction correction is tedious because of the fact that the refraction angular offset changes with azimuthal angle, figuring out which axis needs to move on the beacon flat is complicated. Furthermore, the need of doing the manual alignments for 6 telescopes on every target slew is too much effort.

An automated alignment solution is implemented as it provides the following advantages: (i) reduces the alignment time so that on-sky time can be used more efficiently for science observations. (ii) the real-time alignments in the background for every few seconds maintain the stability of the beam.

5.2 The differential wavelength refraction offset feedback measuring sensors and correction actuators

The STST (infrared, J/H-bands) or the SPICA (visible, R-band) star tracker are used to measure the refraction offset between the LABAO beacon wavelength and the science beam combiner wavelength.

This measured refraction is corrected by moving the LABAO beacon flat actuator.

The optomechanical drifts are measured using the LABAO, STST, and SPICA star tracker and they are corrected using the M7 actuator.

The beacon flat and M7 actuators are mounted on stepper motors. They are controlled by R256 and CHARA inbuilt stepper controllers.

5.3 Automation steps

The alignment to the star is done in four major steps.

1. Slew to star: the telescope is moved to the target coordinates.

2. Co-align of the LABAO and TELAO: this step is semi-automated. The co-alignment is achieved with the blue and red beacons. The process involves a few checkups from the operator such as making sure the alignment is OK before moving to the next steps.

3. Differential refraction correction: We correct the differential wavelength refraction by moving the LABAO beacon flat actuator, which co-aligns the beacon and starlight by correcting the refraction offset. This means the infrared starlight is centered on the expected beam combiner reference fiber position. The LABAO servo stays locked during this process so that M7 can move to keep the blue beacon aligned with the lab WFS. The refraction offset depends on the wavelength and telescope orientation, for example, elevation and azimuth (see Figure). For the infrared beam combiners, the STST sensor is used to measure the refraction angular offset. This STST offset is sent to the beacon flat actuator. For the SPICA, we can use the internal star tracker inbuilt.

4. Optomechanical drifts: corrected by moving the M7 actuator by using the feedback from the LABAO, STST, and SPICA Star tracker.

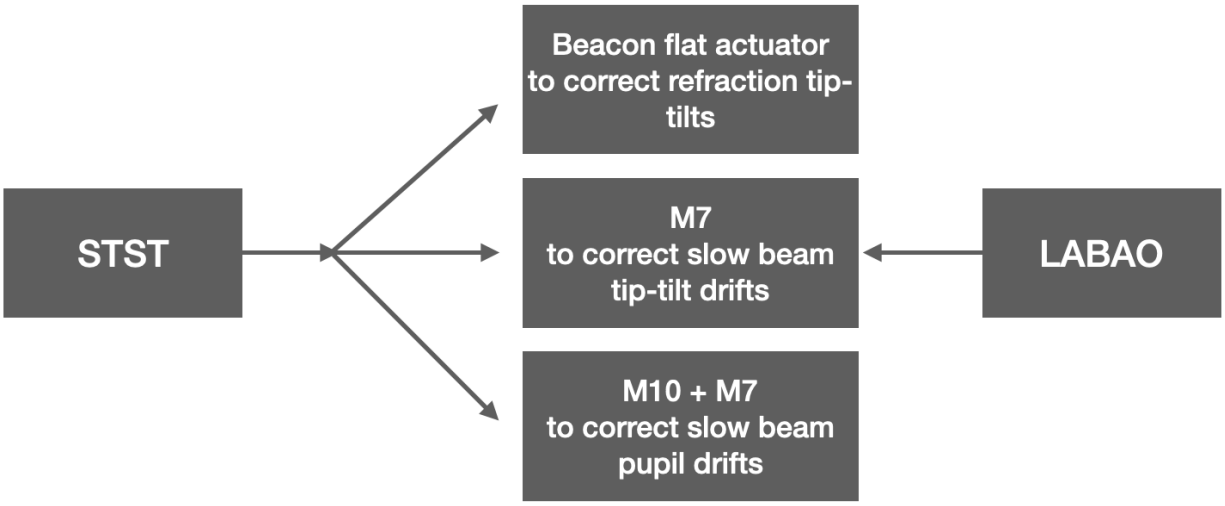

Fig 7 The automatic alignment software is basically a communication between several servers. It gathers information from optical detectors such as LABAO, TELAO, STST, and SPICA star tracker, and converts their coordinates into command control via interaction matrices. This computation also involves the azimuth rotation.

5.4 Software architecture

The LABAO server (e.g. `LABAO_S1`) gathers the STST (`stst_server`) and SPICA star tracker beam tilt and pupil positions and moves the LABAO beacon flat and M7 actuators via `hut server`. The software was developed using the CHARA software architecture, which works as a client/server model.

The automatic alignment algorithm:

- Takes the STST $(x - x_0, y - y_0)$ positions and converts them into the LABAO coordinates
- Takes the SPICA star positions and converts them into the LABAO coordinates
- The LABAO coordinates are then rotated based on the telescope azimuth rotation matrix
- Moves the beacon flats to correct differential wavelength refraction
- Waits 10sec between two consecutive beacon flat moves, to recover the LABAO spots using the M7 correction
- Checks to see if the set points are reached with $\sqrt{((x_0 - x)^2 + (y_0 - y)^2)} < 0.5$ PSF size (2.5) pixels of the STST to call auto alignment complete to finish.
- If the above condition is not reached, it gives up. The operator will decide whether to repeat.

Similar algorithm for the correction optomechical alignment with M7 actuator and LABAO/STST as optical feedback system.

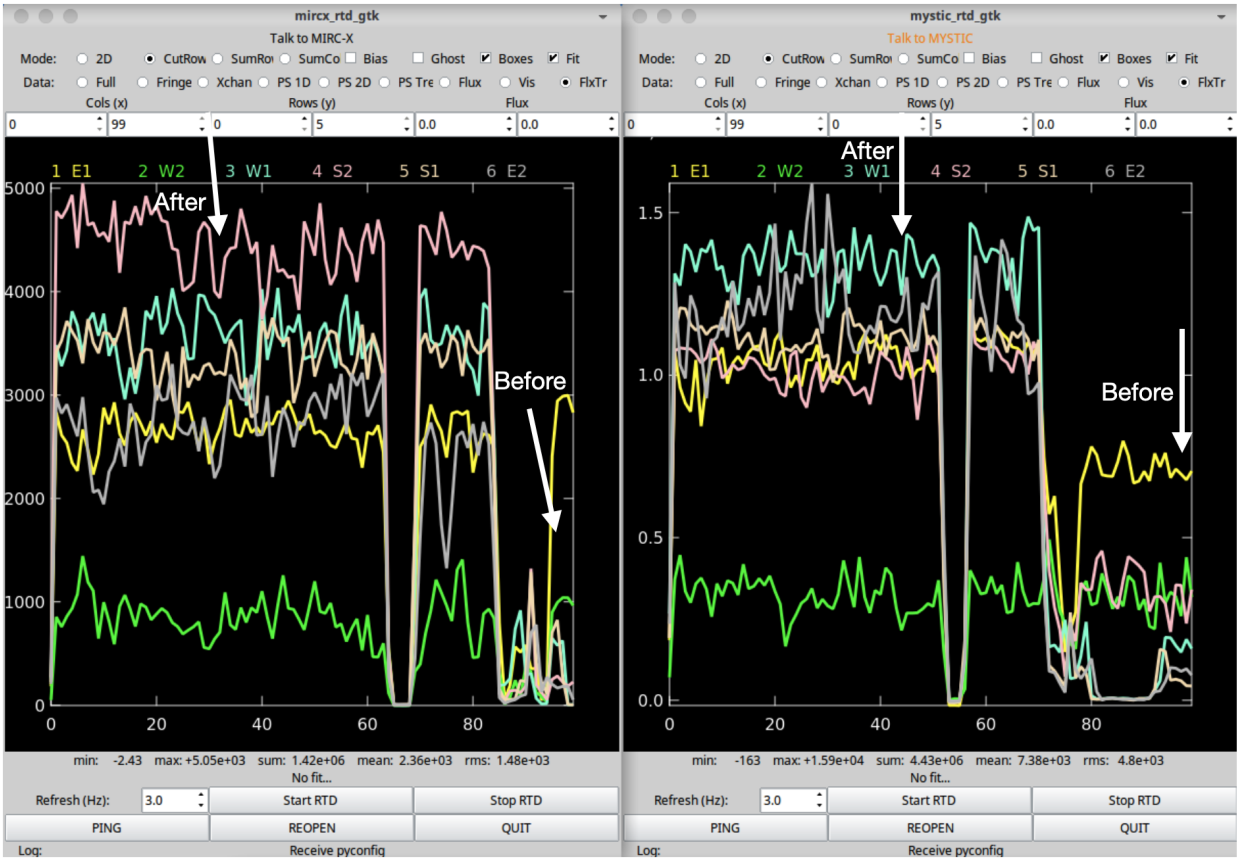

Fig 8 A flux comparison on MIRC-X/MYSTIC on HD 186675. After the refraction affects are corrected the flux is improved. The flux level "before" and "after" refraction correction are shown. A factor of 2-10 flux improvements can be seen, except E1.

5.5 Results

We use the automated alignment software every night at the CHARA Array. The differential wavelength refraction and optomechanical drift correction improve the flux a minimum of $2-10\times$. Figure 8 shows an observation of flux improvement.

6 Discussion

6.1 Alignment systems that work at contemporary interferometers

Checking our works with other contemporary observatories is a good way if we are doing competitively OK. Our STST/SPICA star tracker is similar to the Infrared Image Sensor (IRIS). IRIS is installed in the VLTI lab that images four VLTI telescope beams in the K-band and tracks beam tilt to stabilize the beamlines for the MATISSE and PIONIER at the VLTI (Haubois et al. 2019). IRIS also diagnoses pupil drift that results from warping in the delay line rails. Our LABAO wavefront sensing is similar to the GRAVITY acquisition and guiding camera wavefront sensing. This camera also monitors (beam tip/tilts and pupil) and stabilizes the beam for GRAVITY.[3]

A quick comparison of our beam stabilization is made with the VLTI. VLTI/GRAVITY experiences misalignments in a range of ~ 60 mas RMS in angular offset (size of PSF) and ~ 5% (0.4m RMS) in lateral pupil both for the 8 m telescopes.[3] With their beam guiding,[3] they stabilize the beams at the level of (10 mas RMS in angular offset, 1/5 of PSF size) and 12 mm RMS later pupil (< 0.2% pupil size). They also correct the pupil longitudinal focus[3] to maintain the 2arcsec field of view at the 8 m at the focus of the beam combiner instrument.

6.2 Proposals to reduce the differential wavelength refraction

The CHARA Array was built through a series of medium size funding grants and so the instrument choices and implementation were made on an bespoke way. Although we do a lot of automation in the alignment process, still the alignment takes 5-15 mins, perhaps due to six telescopes, six 2× AO telescopes, and additional auto-alignment corrections. We are thinking of several ideas to improve the alignment time. All these ideas are in the direction of minimizing the differential wavelength refraction. A few are:

1. Low wedge TELDICH: Replacing the current TELDICH with low wedge angle dichroic to reduce refraction effects.

2. Atmospheric dispersion corrector (ADC): Building an atmospheric dispersion corrector at the telescope would be an ideal solution for this dispersion problem. The ADC would with a cost of extra 4 air-glass dioptric surfaces (two Risley prisms) and also optics cost. If we build the ADC, we also need to consider the wedge of the dichroic and vacuum window glass. Maybe high-reflecting coating mirrors (99%) mirrors with gold coating can be selected but need to check if they work for the visible wavelengths.

3. Optimized LABAO beacon wavelength: Choosing the correct beacon wavelength is tricky as there is no optimal solution because we operate both the visible (SPICA, R-band) and near-infrared (MYSTIC, K-band) wavelengths. The 465 nm wavelength LABAO beacon was chosen so that it does not fall in any used science bands. Now as we experience the strong refraction effects, we are considering the idea of replacing the blue beacon (465 nm) with a 1μm (or close) in between the SPICA and MIRC-X wavelengths so that the refraction effects are considerably smaller. This wavelength change means the LABAO systems need to be upgraded as the current camera does not have the sensitivity (see Figure 6 for the sensitivity of the cameras). Also, some of the cameras require a Notch filter to suppress the new LABAO beacon wavelength light. This wavelength operation would be similar to the previous operation of LAB-TIPTILT,[15] which some people argue that it worked with less refraction problems.

6.3 Software improvements

With gaining experience, we are planning to make the auto-alignment faster. We are planning to develop the pupil guiding with the STST pupil monitoring and M10 actuator correction.

6.4 Concluding remarks

We report here a working auto-alignment system, which improves the sensitivity a factor $2-10\times$ of the interferometer and hopefully better visibility measurements. The purpose of this report is to provide a solid reference for technical people for a quick review and also to inspire future instruments in optical interferometry.

Acknowledgments

Most of the ideas and computations are copied from the emails and put together here. Thanks to all the contributors.

References

1 T. A. ten Brummelaar, H. A. McAlister, S. T. Ridgway, *et al.*, "First Results from the CHARA Array. II. A Description of the Instrument," *ApJ* **628**, 453–465 (2005).

2 T. S. Boyajian, K. von Braun, G. van Belle, *et al.*, "Stellar Diameters and Temperatures. II. Main-sequence K- and M-stars," *ApJ* **757**, 112 (2012).

3 N. Anugu, A. Amorim, P. Gordo, *et al.*, "Methods for multiple-telescope beam imaging and guiding in the near-infrared," *MNRAS* **476**, 459–469 (2018).

4 T. Gardner, J. D. Monnier, F. C. Fekel, *et al.*, "ARMADA. I. Triple Companions Detected in B-type Binaries α Del and ν Gem," *AJ* **161**, 40 (2021).

5 C. Lanthermann, T. ten Brummelaar, P. Tuthill, *et al.*, "Design of the new CHARA instrument SILMARIL: pushing for the sensitivity of a 3-beam combiner in the H- and K-bands," in *Optical and Infrared Interferometry and Imaging VIII*, A. Mérand, S. Sallum, and J. Sanchez-Bermudez, Eds., *Society of Photo-Optical Instrumentation Engineers (SPIE) Conference Series* **12183**, 121830N (2022).

6 N. Anugu, J.-B. Le Bouquin, J. D. Monnier, *et al.*, "MIRC-X: A Highly Sensitive Six-telescope Interferometric Imager at the CHARA Array," *AJ* **160**, 158 (2020).

7 B. R. Setterholm, J. D. Monnier, J.-B. Le Bouquin, *et al.*, "MYSTIC: a high angular resolution K-band imager at CHARA," in *Optical and Infrared Interferometry and Imaging VIII*, A. Mérand, S. Sallum, and J. Sanchez-Bermudez, Eds., *Society of Photo-Optical Instrumentation Engineers (SPIE) Conference Series* **12183**, 121830B (2022).

8 D. Mourard, P. Berio, C. Pannetier, *et al.*, "CHARA/SPICA: a new 6T instrument for the CHARA Array," in *Optical and Infrared Interferometry and Imaging VIII*, A. Mérand, S. Sallum, and J. Sanchez-Bermudez, Eds., *Society of Photo-Optical Instrumentation Engineers (SPIE) Conference Series* **12183**, 12183–7 (2022).

9 T. A. ten Brummelaar, L. Sturmann, J. Sturmann, *et al.*, "Adaptive optics for the CHARA array," in *Adaptive Optics Systems III*, B. L. Ellerbroek, E. Marchetti, and J.-P. Véran, Eds., *Society of Photo-Optical Instrumentation Engineers (SPIE) Conference Series* **8447**, 84473I (2012).

10 X. Che, L. Sturmann, J. D. Monnier, *et al.*, "Optical and Mechanical Design of the CHARA Array Adaptive Optics," *Journal of Astronomical Instrumentation* **2**, 1340007 (2013).

11 X. Che, L. Sturmann, J. D. Monnier, *et al.*, "The CHARA array adaptive optics I: common-path optical and mechanical design, and preliminary on-sky results," in *Adaptive Optics Systems IV*, E. Marchetti, L. M. Close, and J.-P. Vran, Eds., *Society of Photo-Optical Instrumentation Engineers (SPIE) Conference Series* **9148**, 914830 (2014).

12 T. A. ten Brummelaar, J. Sturmann, L. Sturmann, *et al.*, "The CHARA array adaptive optics program," in *Adaptive Optics Systems VI*, L. M. Close, L. Schreiber, and D. Schmidt, Eds., *Society of Photo-Optical Instrumentation Engineers (SPIE) Conference Series* **10703**, 1070304 (2018).

13 N. Anugu, T. ten Brummelaar, N. H. Turner, *et al.*, "CHARA array adaptive optics: complex operational software and performance," in *Society of Photo-Optical Instrumentation Engineers (SPIE) Conference Series*, *Society of Photo-Optical Instrumentation Engineers (SPIE) Conference Series* **11446**, 1144622 (2020).

14 H. G. Roe, "Implications of Atmospheric Differential Refraction for Adaptive Optics Observations," *PASP* **114**, 450–461 (2002).

15 L. Sturmann, J. Sturmann, T. ten Brummelaar, *et al.*, "Nine-channel tip/tilt detector at the CHARA Array," in *Advances in Stellar Interferometry*, J. D. Monnier, M. Schöller, and W. C. Danchi, Eds., *Society of Photo-Optical Instrumentation Engineers (SPIE) Conference Series* **6268**, 62683T (2006).